CIRP Annals - Manufacturing Technology 00 (2025) 1–5

Contents lists available at ScienceDirect

CIRP Annals - Manufacturing Technology

journal homepage: https://www.editorialmanager.com/CIRP/default.aspx

Circular manufacturing of binder jetting additive parts from Ti-6Al-4 V machining chips

Debajyoti Bhaduri[a,*], Karan A. Baramate[a], Soumya Gangopadhyay[b], Thomas E. Davies[c]

[a] High-Value Manufacturing Research Group, School of Engineering, Cardiff University, Cardiff, United Kingdom
[b] Department of Mechanical Engineering, Indian Institute of Technology Bhilai, Durg, Chhattisgarh, India
[c] Cardiff Catalysis Institute, School of Chemistry, Cardiff University, Cardiff, United Kingdom

Submitted by T.H.C. Childs (1), Leeds, UK

ARTICLE INFO

Article history:
Available online xxx

Keywords:
Binder jetting
Titanium
Ball milling

ABSTRACT

The viability of using ball milled (BM) Ti-6Al-4V machining chips for fabricating parts by binder jetting (BJT) additive manufacturing is reported. The built parts' density, roughness, microhardness and compressive strength are compared with BJT parts made from gas atomised (GA) powder. Sintered BM and GA parts exhibit comparable relative density (93–95 %), while microhardness of the former is almost twice of the latter. Equiaxed grains with greater β-phase fraction are observed in the BM parts' microstructure. The BM compression test pieces exhibit brittle fracture due to greater strain hardening of the BM particles, compared to the plastic deformation of the GA specimens.

1. Introduction

Today, circular economy models in manufacturing are increasingly being adopted via material recycling, reduction of energy consumption and energy recovery [1], to meet United Nation's Sustainable Development Goals. For the additive manufacturing (AM) sector, despite the immense benefits offered by the AM technology in terms of design freedom and material waste reduction [2], conventional AM powder production routes involving melting and atomisation processes (such as gas, water and plasma atomisation) consume substantial energy and have high carbon footprint. To mitigate this, reuse of commercial powders [3] as well as alternative powder generation routes via solid-state crushing of machining chips have been explored. For powder metallurgy (PM) application, Teja et al. [4] explored the possibility of recycling titanium (Ti) chips, mixed with graphite (C) powders when ball milling (BM). The produced in-situ Ti-TiC composite powders were utilised for fabricating pellets via sintering and compaction. In relation to the AM application, irregular shaped BM 304L and Ti-6Al-4V particles have been used to deposit single tracks via laser engineered net shaping [5] and direct metal laser sintering [6] processes, respectively. In both cases, the BM particles exhibited higher hardness compared to the machining chips due to the greater dislocation density and grain refinement of particles caused by the work hardening effect during BM. In the context of part fabrication, mechanically generated 316L feedstock has been utilised to build tensile bars via a directed energy deposition (DED) AM process [7]. The resulting tensile specimens showed presence of interstitial elements (e.g., oxygen and Ti). These led to marginally higher hardness, Young's modulus, ultimate tensile strength and yield strength, but lower elongation at fracture, compared to values from spherical gas atomised powder parts. In the case of DED-printing of tensile pieces from AISI 303 chip powder on an AISI 1045 substrate failure occurred in the substrate region, indicating a good adhesion between the two materials [8]. Direct feeding of machining chips and grinding swarf into DED process has also been tested, without converting them into powders [9–11]. It was concluded that prior chip cleaning is not required as impurities are burnt off during the laser melting of the DED process [10].

Up to now the main reported uses [7–11] of mechanically-generated feedstock have been with DED processes (powder feeding is more simple with DED than with powder bed fusion (PBF) and binder jetting (BJT) AM processes). The reporting of chip powder as feed for PBF or BJT processes is extremely limited. The BJT AM process is similar in its working principles to powder metallurgy. Since chip powders have demonstrated potential as alternative feedstock for PM [12], a research need is to evaluate the viability of using such powder particles in BJT process. This research centres on the fabrication and testing of BJT test pieces from ball milled Ti-6Al-4V (Ti64) chip powder via a circular manufacturing process chain, as shown in Fig. 1.

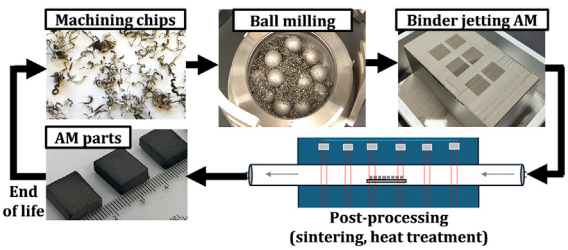

Fig. 1. A schematic of the circular manufacturing process chain.

* Corresponding author.
E-mail addresses: debajyoti.bhaduri@gmail.com, BhaduriD@cardiff.ac.uk (D. Bhaduri).

https://doi.org/10.1016/j.cirp.2025.03.037

The purpose of the paper is to compare the fabricated parts' surface and mechanical integrity against those built using commercial gas atomised (GA) Ti64 powder.

2. Experimental methodology

Ti64 chips of length ~1–30 mm, width 1.2±0.9 mm and thickness 0.17±0.16 mm were generated from ASTM B265 Grade 5 annealed plates, using standard wet end milling conditions (95 m/min cutting speed, 0.5 mm/rev feed and 0.2 mm depth of cut). The chips were ultrasonically cleaned using detergent, acetone and isopropyl alcohol, for 15 mins for each cycle, and finally dried in an oven for 2 h at 120 °C to remove moisture. BM of clean chips was then carried out in a Retsch PM400 ball miller, using four 250 mL hardened chrome steel grinding jars. As recommended in [5], a two-stage BM process was undertaken. Following comprehensive trials the final BM parameters are shown in Table 1. After Stage 1, BM particles with <150 µm average size were sieved and utilised in Stage 2, following which, particles with <100 µm size were sieved and used for BJT printing.

Table 1
Two-stage ball milling parameters for Ti-6Al-4V chips

BM stages	Ball-to-powder ratio	Ball dia. (mm)	Jar vol. (mL)	BM RPM	BM run time (min)
Stage 1	20:1	20	250	300	90
Stage 2	10:1	10	250	250	60

Fabrication of BJT cubes (12 × 10 × 6 mm) and compression test pieces (Φ10 × 10 mm) from commercial GA and BM powders was conducted on an ExOne Innovent+ machine, using CleanFuse binder. Due to the limited quantity of the BM powder, miniaturised compression test pieces were built as per [13]. Standard printing conditions (shown in Table 2) were used, as recommended by ExOne. The printed 'green parts' were cured in an oven at 140 °C for 6 h. Debinding and 'pressure-less' sintering of the cured cubic parts were then undertaken in a CM 1630–20 horizontal tube furnace in an argon atmosphere. Debinding was carried out at 550 °C for 1 h. Three sintering cycles at 1290, 1390 and 1490 °C, each for a duration of 2 h [14], followed by furnace cooling, were initially tested. Based on the sintered cubes' density, roughness and surface topography results, a final sintering cycle of 1490 °C for 3 h was chosen for sintering further cubic and compression test pieces.

Table 2
Binder jetting, curing and sintering parameters used

Binder saturation	80 %
Layer thickness	50 µm
Binder droplet volume	30 pL
Build bed drying temperature	60 °C
Green parts' curing cycle	140 °C, for 6 h
Trial sintering cycles	1290, 1390, 1490 °C, for 2 h
Final sintering cycle	1490 °C, for 3 h

Particle size distribution analysis was carried out using a vibratory sieve shaker, according to ASTM B214–16. Powder flowability was evaluated using a Hall flowmeter, according to ASTM B213–17. The GA and BM particle morphology and sintered parts' surface topography were observed using a scanning electron microscope (SEM). Relative density was measured twice on each sintered specimen using Archimedes principle. Surface roughness parameters, Sa and Sz, were recorded using a Sensofar 3D optical profilometer on a 1.7 × 1.4 mm^2 area with a 0.8 mm nesting index. The average values of three measurements on each of the three samples per sintering cycle are presented. Vickers microhardness measurements were carried out on the polished cross-sections of the cubes along the printing (X-Y plane) and the build (Y-Z plane) directions (see Fig. 4(a)), with 100 g load and 10 s dwell time. The average values of five measurements on each plane are displayed. Microstructures were revealed via immersion etching in Kroll's reagent (100 mL water, 3 mL hydrofluoric acid, 6 mL nitric acid) for 1 min. Electron backscatter diffraction (EBSD) analysis was further undertaken to evaluate the grain size and phase fraction. Additionally, phase detection was carried out using X-ray diffraction with a Cu-Kα target, 0.02° step size, and 1.2 s/step scan speed, within a 2θ range of 30°-80°.

Compression tests were carried out on three GA and three BM BJT test pieces using a constant displacement rate of 0.5 mm/min at ambient temperature [14].

3. Results

3.1. Physical and mechanical results

The commercial GA powder exhibited spherical morphology with particle size between ~15–45 µm, shown in Fig. 2(a). The machined Ti64 chips were mainly segmented, but some were up to ~30 mm long, displayed in Fig. 2(b). The optimised two-stage BM process was able to crush all chips and produced irregular shaped particles (Figs. 2(c) and 2(d)), similar to that reported in [6,15]. A two-stage BM cycle converted ~98 % of the initial chip mass into 80 g of particles with <100 µm average size in a BM run time of 2.5 h and a total milling time of 4 h 40 mins, including the 10 mins machine pause time after each 10 mins of BM run time. After 13 two-stage BM cycles, a total 1 kg of powder with <100 µm particle size was used for BJT printing. Fig. 3 shows that the angle of repose (AOR=31°) of 50 g BM powder was marginally higher than its GA counterpart (28°), possibly due to the greater size distribution of the BM particles, ~5–100 µm. Nonetheless, the flowability test confirmed that the BM powder was 'free flowing'.

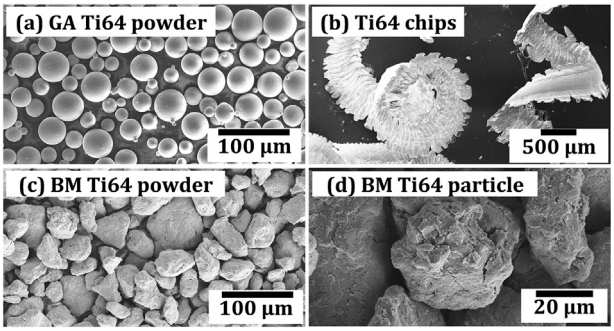

Fig. 2. SEM micrographs of Ti64 chips, GA and BM powder particles.

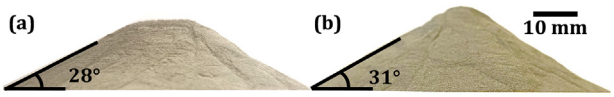

Fig. 3. Hall flowability test, (a) GA powder, (b) BM powder.

Fig. 4(a) shows a 'green' part printed from BM powder. X-Y is the printing plane with the Z-axis as the build direction. Figs. 4(b) and 4(c) are BM and GA parts sintered at 1490 °C for 3 hrs. Fig. 4(d) is a 'green' compression test piece printed using BM powder. Fig. 4(e) shows its counterpart sintered at 1490 °C for 3 h.

Relative densities of both the GA and BM BJT 'green' parts were ~55–60 %. Densification started at a lower sintering temperature for the GA than the BM parts. Fig. 4(f) shows densification over the sintering range 1290 °C to 1490 °C and 2 to 3 h. Sintering of BM parts only started near to 1390 °C and 2 h but both the BM and GA parts that were sintered at 1490 °C and 2 h repeatedly achieved 93–94 % relative density. Further increase in sintering temperature was not possible due to the furnace's capacity. However, increasing the sintering time from 2 h to 3 h marginally increased both GA and BM parts' density to 93–95 %, possibly due to the grain growth. Although the density is lower than with PBF parts, where 98–99 % part density is achievable, the BJT part densities are comparable with prior work [14,16].

As seen from Fig. 4(g), average surface roughness, Sa and 10-point roughness, Sz of both GA and BM parts decreased with the rise of sintering temperature, due to improved densification and bonding of

Please cite this article as: D. Bhaduri et al., Circular manufacturing of binder jetting additive parts from Ti-6Al-4 V machining chips, CIRP Annals - Manufacturing Technology (2025), https://doi.org/10.1016/j.cirp.2025.03.037

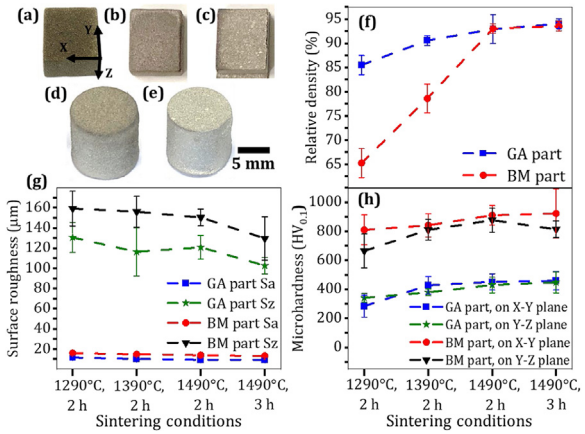

Fig. 4. (a) BM 'green' part, (b) BM sintered part, (c) GA sintered part, (d) BM 'green' and (e) BM sintered compression test pieces, (f) relative density, (g) surface roughness and (h) microhardness of GA and BM parts.

particles. Sa of the GA and BM cubes were in the range of 8–12 and 12–15 μm, respectively, following sintering at 1490 °C for 3 h. The BM parts exhibited ~10–30 % higher Sa and ~20–25 % greater Sz compared to the GA parts. Fig. 5 adds to the surface roughness information. Fig. 5(a) shows the smaller particle sizes (<50 μm) of the GA surface relative to those of the BM surface (<100 μm, Fig. 5(c)). The enlarged views, Figs. 5(b) and 5(d) show the smoother material flow under surface tension of the GA part surfaces compared to the still visually individually sintered and bonded BM part surfaces.

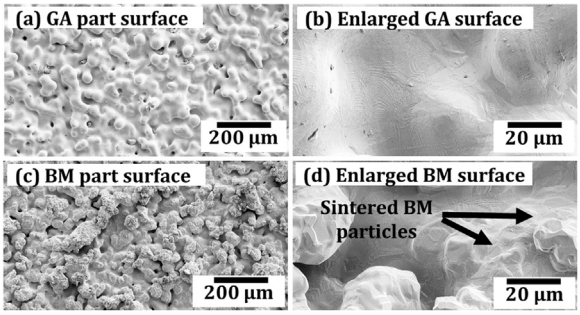

Fig. 5. Surface topography of GA and BM parts, sintered at 1490 °C, 3 h.

Fig. 4(h) shows that microhardness of both GA and BM parts increased with the increase in sintering temperature, in line with parts' densification and reduction of internal pores (Section 3.2). Microhardness values recorded on the X-Y plane were generally higher than those measured on the Y-Z plane. This was possibly because better bonding between particles took place along the plane of printing than that along the build direction. Nonetheless, the difference was marginal when sintering at 1490 °C. In this condition, average microhardness of the GA part (450–460$HV_{0.1}$) was higher than the wrought Ti64 blocks (350$HV_{0.1}$) that were purchased off-the-shelf to produce BM powder. The value was also substantially higher than hardness of as-sintered Ti64 BJT part (336HV) reported in [17]. Interestingly, the BM parts exhibited ~810–920$HV_{0.1}$ average hardness when sintered at 1490 °C which is almost twice the hardness of the GA parts.

Fig. 6 depicts that the compressive yield strength of three tested GA specimens was in the range of 910–1000 MPa, while the strain at failure was of the order of ~22–28 %. The yield strength was 6–16 % higher but the failure strain was substantially greater than that reported in [14], i.e. 862 MPa and 3.7–4 %, respectively. Indeed, one GA test piece was plastically deformed without breakage as shown in Fig. 6(a). In contrast, the BM test pieces' compressive strengths were from 510–870 MPa, with near-brittle failure (failure strains <3 %). Brittle fractures along the grain boundaries, along with tiny lateral cracks are seen in Fig. 6(b).

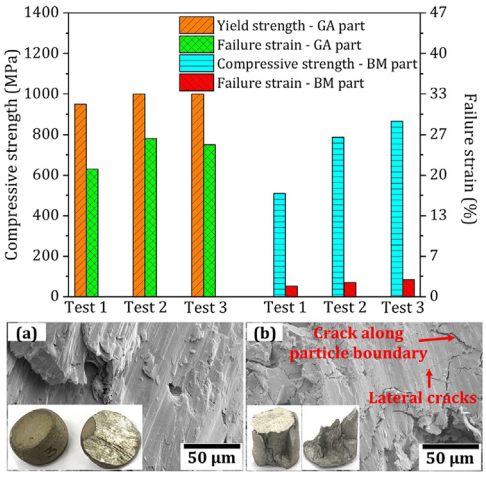

Fig. 6. Compressive yield strength and failure strain results, together with the failure regions of (a) GA parts and (b) BM parts.

3.2. Microstructural observations

The microstructure of the wrought Ti64 block in Fig. 7(a) shows typical partly equiaxed and elongated primary α colonies, together with intergranular lamellar α/β phases. The machining process deformed the α grains within the chips, together with distorted α/β phases, as seen in Fig. 7(b). In Fig. 7(c), the BJT GA part exhibits basket-weave structures of lamellar α within the prior β grains as the part was sintered well above the β-transus (995 °C for Grade 5 Ti64) and furnace cooled. Some pores and needle-like thin β grains are also visible. Similar structures are reported in [17,18]. EBSD analysis on the GA part confirms the presence of lamellar grains in the inverse pole figure (IPF), shown in Fig. 8(a). The corresponding phase map in Fig. 8(b) shows the matrix is nearly fully hexagonal α, with marginal cubic β phases mainly accumulated within the needle-like structures. Energy dispersive spectroscopy (EDS) detected these regions as vanadium (V)-rich, which is a β-stabiliser, confirming the presence of β phases.

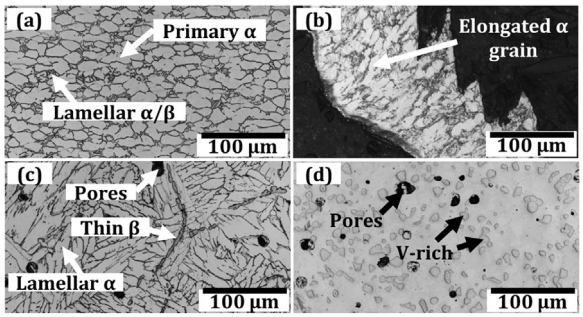

Fig. 7. Microstructures of (a) wrought Ti64 block, (b) machined chip, (c) BJT GA part and (d) BM part, sintered at 1490 °C for 3 h.

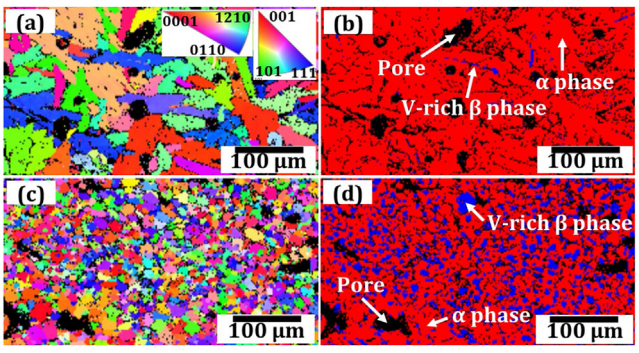

Fig. 8. EBSD IPF of (a) BJT GA part and (b) its phase map, (c) IPF of BJT BM part and (d) its phase map. Both parts sintered at 1490 °C for 3 h.

Please cite this article as: D. Bhaduri et al., Circular manufacturing of binder jetting additive parts from Ti-6Al-4 V machining chips, CIRP Annals - Manufacturing Technology (2025), https://doi.org/10.1016/j.cirp.2025.03.037

In contrast to the microstructure of the GA part, the BJT BM part shows fine nearly globular dark phases dispersed throughout the matrix, together with some pores in Fig. 7(d).

EDS detected these dark phases as V-rich. The corresponding EBSD IPF in Fig. 8(c) reveals fine equiaxed grains of ~5–25 µm. The phase map in Fig. 8(d) confirms that the fine dark phases are indeed cubic β phases. The presence of a higher β fraction in BJT BM parts can be attributed to the prior higher volume fraction of β in the BM particles that occurred due to the strain hardening of Ti64 chips during ball milling. It is reported that β-phase fraction increases with an increase in strain due to vanadium depletion from the supersaturated α. The rise in V percentage at new sites promotes fresh formation of intergranular β [19]. The higher hardness of the BM parts reported earlier is due to the greater β fraction [20], coupled with the prior work hardening of the BM particles [5,6] and smaller grain size of the BM parts, as per Hall-Petch relation.

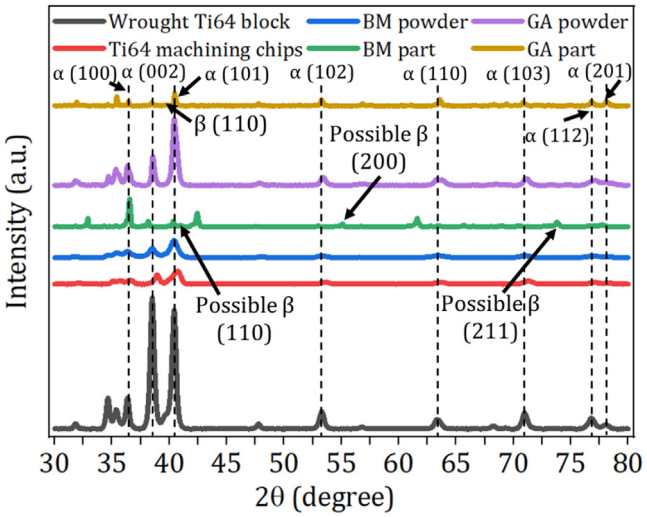

Fig. 9. X-ray diffraction spectra of wrought Ti64 block, Ti64 chips, BM and GA powders and BJT parts.

The XRD spectra in Fig. 9 shows that α-Ti phase exists as the main crystalline peaks in all specimens. Some possible β peaks in the BM part are also indicated. The tiny β (110) peak seen at 40° diffraction angle [21] might also coincide with the peak of TiC [14]. There is a possibility of formation of some TiC and titanium oxides within the parts as BJT printing was carried out in atmospheric condition. Traces of carbon and nitrogen have also been detected via EDS on both GA and BM parts, however, the relative percentages of C and N were 3–5 wt % higher in some regions of the latter specimens. This is expected as the BM powder was generated in atmospheric condition whereas the GA powder was supplied in an argon-sealed container.

4. Discussion

The study involved different batches of Ti64 chips generated from several Grade 5 annealed plates. Chips with varied length (~1–30 mm) were successfully converted into powder particles via ball milling. Using the optimised two-stage BM settings, ~98–99 % of the initial chip mass was transformed into particles with <100 µm average size in a BM run time of 2.5 h. This was substantially lower than the long BM durations found in literature, e.g., 2.5–12 h in [4], 24–60 h in [5], and 6–18 h in [6]. Each two-stage BM cycle, involving four 250 mL jars, produced 80 g powder. Of all the BM powder produced and used for BJT printing, the average size of 25–35 wt % of particles was <50 µm and 65–75 % was 50–100 µm. Thus, the process can be scaled up by using larger milling jars and by operating machines in parallel.

The irregular shaped particles, generated via solid-state crushing, can be successfully used in BJT printing as the powder is first laid and then compacted by two rollers. The greater size distribution (~5–100 µm) could also help in filling in the voids between larger particles. Despite the irregular shape, the BM powder was 'free flowing' [22], consistently exhibiting 29.5°-34° static AOR, compared to the 26°-31° AOR of the GA powder. While such irregular BM particles displayed a turbulent flow behaviour in a DED process and produced layers with pores of varying size [15], in the present study, both BJT BM and GA parts sintered at 1490 °C for 3 h achieved 93–95 % relative density consistently. However, the greater particle size distribution and irregular shape also resulted in the 10–30 % higher Sa of the BM surfaces, compared to the GA surfaces. A fine equiaxed microstructure with higher cubic β fraction was observed on the BM parts, compared to the lamellar microstructure of the GA parts containing greater fraction of hexagonal α phase. Equiaxed microstructure of DED tracks deposited using BM powder was also reported in [15]. The reason was attributed to the grain refinement due to ultrasonic cavitation of molten melt pool. In contrast, the equiaxed microstructure in the present study is thought to be due to prior strain hardening of the BM particles and consequent formation of greater β-phase fraction.

The microhardness of the BM parts was almost twice that of the GA parts, though their compressive strength was less than that of the GA parts' yield strength, and they failed in an almost brittle manner. The higher hardness is believed to arise from the combined effects of the strain hardening and greater β fraction of the BM powder. The strain hardening, together with higher traces of impurities (C, N) in the powder, induced during ball milling, are possible causes of their lower malleability. Nonetheless, the highest compressive strength recorded for the BM specimens (866 MPa) was comparable to that reported in [14]. Conversely, the presence of fully lamellar hexagonal α was the contributing factor for the greater malleability of the GA parts.

5. Conclusions

Mechanically-generated powder can be used successfully to build parts by the binder jetting AM process. The parts built from ball milled powder have similar relative density (93–95 %) to parts built from GA commercial powder but have higher hardness and are less malleable. Fine equiaxed grains, with greater β-phase fraction, are observed in the BM parts' microstructure. It is believed that the prior strain hardening of the BM particles is in part the cause of the higher hardness and lower malleability.

Future research will focus on further improving the density of the BJT parts via post-processing, for example, hot isostatic pressing [17]. Post-BJT heat treatment routes will be explored to enhance the ductility/malleability of the BM parts.

Declaration of competing interest

The authors declare that they have no known competing financial interests or personal relationships that could have appeared to influence the work reported in this paper.

CRediT authorship contribution statement

Debajyoti Bhaduri: Writing – original draft, Supervision, Project administration, Funding acquisition, Conceptualization. **Karan A. Baramate:** Investigation, Formal analysis, Data curation. **Soumya Gangopadhyay:** Writing – review & editing, Supervision, Funding acquisition. **Thomas E. Davies:** Writing – review & editing, Resources.

Acknowledgments

We acknowledge the Indian Government's Scheme for Promotion of Academic and Research Collaboration (SPARC) grant.

Supplementary materials

Supplementary material associated with this article can be found, in the online version, at doi:10.1016/j.cirp.2025.03.037.

References

[1] Kara S, Hauschild M, Sutherland J, McAloone T (2022) Closed-loop systems to circular economy: A pathway to environmental sustainability? *CIRP Annals - Manufacturing Technology* 71:505–528.
[2] Thompson KA, Moroni G, Vaneker T, Fadel G, Campbell RI, Gibson I, Bernard A, Schulz J, Graf P, Ahuja B, Martina F (2016) Design for additive manufacturing: trends, opportunities, considerations, and constraints. *CIRP Annals - Manufacturing Technology* 65:737–760.
[3] Terrassa KL, Haley JC, MacDonald BE, Schoenung JM (2018) Reuse of powder feedstock for directed energy deposition. *Powder Technol* 338:819–829.
[4] Teja PJ, Shial SR, Chaira D, Masanta M (2020) Development and characterization of Ti-TiC composites by powder metallurgy route using recycled machined Ti chips. *Materials Today: Proceedings* 26:3292–3296.
[5] Fullenwider B, Kiani P, Schoenung JM, Ma K (2019) Two-stage ball milling of recycled machining chips to create an alternative feedstock powder for metal additive manufacturing. *Powder Technol* 342:562–571.
[6] Dhiman S, Joshi RS, Singh S, Gill SS, Singh H, Kumar R, Kumar V (2022) Recycling of Ti6Al4V machining swarf into additive manufacturing feedstock powder to realise sustainable Recycling goals. *J Clean Prod* 348:131342.
[7] Jackson MA, Morrow JD, Thoma DJ, Pfefferkorn FE (2020) A comparison of 316 L stainless steel parts manufactured by directed energy deposition using gas-atomized and mechanically-generated feedstock. *CIRP Annals - Manufacturing Technology* 69:165–168.
[8] Castanheira L, Gil J, Amaral R, Vieira T, Reis A, Emadinia O (2024) Parametrization and characterization of DED printings using recycled AISI 303 powder particles. *Powder Technol* 435:119453.
[9] Mahmood K, Ul Haq Syed W, Pinkerton AJ (2011) Innovative reconsolidation of carbon steel machining swarf by laser metal deposition. *Opt Lasers Eng* 49:240–247.
[10] Murray JW, Speidel A, Jackson-Crisp A, Smith PH, Constantin H, Clare AT (2021) Unprocessed machining chips as a practical feedstock in directed energy deposition. *International Journal of Machine Tools and Manufacture* 169:103803.
[11] Dhami HS, Panda PR, Viswanathan K (2022) Production of powders for metal additive manufacturing applications using surface grinding. *Manufacturing Letters* 32:54–58.
[12] Batista CD, de Pinho Fernandes AAN, Vieira MTF, Emadinia O (2021) From machining chips to raw material for powder metallurgy - A review. *Materials (Basel)* 14:5432.
[13] Iyibilgin O, Gepek E (2021) Characterization of CP-titanium produced via binder jetting and conventional powder metallurgy. *Revista De Metalurgia* 57(4):e205.
[14] Tang Y, Huang Z, Yang J, Xie Y (2020) Enhancing the capillary force of binder-jetting printing Ti6Al4V and mechanical properties under high temperature sintering by mixing fine powder. *Metals (Basel)* 10:1354.
[15] Wolff S, Haddad M, Zhang J, Luo A (2024) Effect of recycled swarf and spherical Ti-6Al-4V feedstocks on laser directed energy deposition additive manufacturing. *CIRP Annals - Manufacturing Technology* 73:193–196.
[16] Simchi A, Petzoldt F, Hartwig T, Hein SB, Barthel B, Reineke L (2023) Microstructural development during additive manufacturing of biomedical grade Ti-6Al-4V alloy by three-dimensional binder jetting: material aspects and mechanical properties. *The International Journal of Advanced Manufacturing Technology* 127:1541–1558.
[17] Alegre JM, Díaz A, García R, Peral LB, Lorenzo-Bañuelos M, Cuesta II (2024) Mechanical and fatigue properties of Ti-6Al-4V alloy fabricated using binder jetting process and subjected to hot isostatic pressing. *Materials (Basel)* 17:3825.
[18] Tischel F, Reineke L, Alrashdan J, Ploshikhin V (2024) Experimental investigation and modeling of densification during sintering of binder jetted Ti-6Al-4V. *Powder Technol* 444:119958.
[19] Souza PM, Hodgson PD, Rolfe B, Singh RP, Beladi H (2019) Effect of initial microstructure and beta phase evolution on dynamic recrystallization behaviour of Ti6Al4V alloy - an EBSD based investigation. *J Alloys Compd* 793:467–479.
[20] Pathania A, Subramaniyan AK, Nagesha B (2022) Influence of post-heat treatments on microstructural and mechanical properties of LPBF-processed Ti6Al4V alloy. *Progress in Additive Manufacturing* 7:1323–1343.
[21] Gupta A, Khatirkar RK, Kumar A, Parihar MS (2018) Investigations on the effect of heating temperature and cooling rate on evolution of microstructure in an $\alpha + \beta$ titanium alloy. *J Mater Res* 33(8):946–957.
[22] Zegzulka J, Gelnar D, Jezerska L, Prokes R, Rozbroj J (2020) Characterization and flowability methods for metal powders. *Sci Rep* 10:21004.

Please cite this article as: D. Bhaduri et al., Circular manufacturing of binder jetting additive parts from Ti-6Al-4 V machining chips, CIRP Annals - Manufacturing Technology (2025), https://doi.org/10.1016/j.cirp.2025.03.037